JAAS

Accepted Manuscript

This is an *Accepted Manuscript*, which has been through the Royal Society of Chemistry peer review process and has been accepted for publication.

Accepted Manuscripts are published online shortly after acceptance, before technical editing, formatting and proof reading. Using this free service, authors can make their results available to the community, in citable form, before we publish the edited article. We will replace this *Accepted Manuscript* with the edited and formatted *Advance Article* as soon as it is available.

You can find more information about *Accepted Manuscripts* in the Information for Authors.

Please note that technical editing may introduce minor changes to the text and/or graphics, which may alter content. The journal's standard Terms & Conditions and the Ethical guidelines still apply. In no event shall the Royal Society of Chemistry be held responsible for any errors or omissions in this *Accepted Manuscript* or any consequences arising from the use of any information it contains.

ROYAL SOCIETY OF CHEMISTRY

www.rsc.org/jaas

High-precision measurements of tungsten stable isotopes and application to Earth Sciences

Thomas Breton*, Ghylaine Quitté*

Laboratoire de Géologie de Lyon, Ecole normale supérieure de Lyon, Université de Lyon, CNRS, UMR 5276, 46 allée d'Italie, F-69364 Lyon cedex, France

* Present address: *Institut de Recherche en Astrophysique et Planétologie, Observatoire Midi Pyrénées, Université de Toulouse, CNRS, UMR 5277, 14 avenue Edouard Belin, F-31400 Toulouse, France*

Abstract

Mass-dependent isotope fractionation of tungsten (W) isotopes has not received much attention until recently. This is mainly due to the small fractionation expected – as tungsten has a relatively high atomic mass – combined with the insufficient precision that could be achieved with the existing techniques. Tungsten is involved in the ^{182}Hf-^{182}W radio-chronometer. Hence, tungsten isotopes are currently mainly used for studying the first stages of the solar system history, as they are well suited to trace metal-silicate equilibration processes. At the same time, evaporation, condensation or diffusion are known to fractionate stable isotopes. A better understanding of W stable isotopes behavior during terrestrial and asteroidal processes will thus potentially shed light on those events. We here present an improved separation procedure based on anion-exchange chromatography that allows achieving quantitative recovery of W. Taking advantage of the last generation multi-collector inductively coupled plasma mass-spectrometers (MC-ICPMS), we also set up a method to analyze W mass-dependent isotope fractionation with an external reproducibility better than 80 ppm and an internal reproducibility of 30 ppm. This new analytical procedure has been applied to igneous and iron-rich samples, from granites to chondrites and iron meteorites. Isotope variations observed for natural samples are well resolvable and vary from -0.05 to +0.36 per mil per mass unit.

1 - Introduction

The study of mass independent fractionation of W isotopes is of great interest for chronological purposes[1–9] and for understanding nucleosynthetic processes and subsequent dynamical processes in the solar nebula[10–12]. The ^{182}Hf-^{182}W chronometer is well-suited to date, for instance, the formation of iron meteorites[2,6,13–15], the metamorphism of H-chondrites[16], or the metal-silicate segregation in achondrites[5,7,8,17–19], thus proving to be useful in understanding the first stages of solar system history and planetary formation. Tungsten isotope measurements are usually performed after separation of W from the matrix elements using an anion-exchange resin, and involve mass spectrometry techniques, be it multi-collector inductively-coupled plasma mass spectrometry[1,6,13,15,16] (MC-ICMPS) or negative ion thermal ionization mass spectrometry[20,21] (N-TIMS).

Stable isotope fractionation provides information about processes, including isotope exchange between phases, and redox reactions. They allow evaluating diffusion temperatures, constraining chemical equilibria and kinetics, and characterizing sources of specific material and reaction pathways. Fractionation of W stable isotopes is potentially of broad interest in both geochemistry and cosmochemistry. It could for instance bring additional constraints on the long-standing search for the origin of reduced metal in chondrites and primitive achondrites. It could also provide new information on metal-silicate phase equilibrium to help unravel the processes involved in the formation of iron meteorites. Additionally, it may clarify the processes related to the moon-forming impact and the late veneer theories. Tungsten stable isotopes may also be used as a tracer of the dissolved minerals in alteration processes, and its solubility makes W stable isotopes suitable for tracing the geographic origin of detritic material.

Recent improvements in mass spectrometry instrumentation push back the frontiers of mass-dependent fractionations and heavy elements such as cadmium[22–25], molybdenum[26] and

thallium[27–30] have been successfully investigated. Thanks to the stability and sensitivity of the new generation Thermo Scientific® *Neptune Plus*© MC-ICPMS and its *Jet Cones* interface, the achievable precision on isotope measurements has significantly improved, a pre-requisite to study heavy elements presenting only small isotope fractionations. In the following, we present a new method for measuring the fractionation of W stable isotopes with high precision.

So far, only one study specifically addressed the question of mass-dependent fractionation of W stable isotopes[31]. In the other studies of W isotope fractionation, the mass-dependent effect is always corrected for during data processing as the measured isotope ratios are internally normalized, i.e. corrected for the mass bias using a stable isotope ratio ($^{186}W/^{183}W$ or $^{186}W/^{184}W$) as reference. This normalization erases all mass-dependent fractionations, be they caused by the ICPMS instrument, by the ion-exchange procedure, or be they intrinsic to the sample.

2 - Sample preparation

2.1 - Reagents and test-solutions

Samples were prepared in a clean room at the Laboratoire de Géologie de Lyon - ENS de Lyon. We used Teflon Savillex© vials for every step of the procedure. Commercial HCl, HF and HNO_3 acids were distilled once (HCl, HNO_3) or twice (HF) in sub-boiling stills. Commercial suprapur H_2O_2 (Merck©) was also used. Reagent blanks are summarized in Table 1. H_2O_2-bearing solutions were always prepared in the hour preceding their use to limit the decomposition of the metastable molecule. Sample handling was performed under a laminar-flow in order to reduce the risk of sample contamination.

Our goal was to set up a procedure suitable for most terrestrial and extraterrestrial rock samples, so that different solutions and natural samples were used throughout our analytical

development: (1) a pure tungsten standard solution (Alfa-Aesar© for ICPMS) to check the procedure yield, (2) the NIST SRM 3163 W isotopic standard to ensure there was no procedure-induced isotope fractionation, (3) a home-made multi-element standard solution as well as (4) W-free terrestrial matrices doped with NIST SRM 3163 to check matrix effects, and finally (5) terrestrial and extra-terrestrial samples.

A multi-element standard solution was prepared from mono-element Alfa-Aesar© standard solutions, as a mixture of the most common major and minor elements found in samples of interest (Na, Mg, Al, K, Ti, Cr, Mn, Fe, Co, Ni, Cu), along with a set of trace elements (Rb, Sr, Mo, Sn, Sb, Ba, REE, Hf, Ta, Re, Os, Pb, Th) including the elements interfering with W (Table 2). Natural matrices were also doped with standard W after removal of the W they initially contained: the W initially present in rock standards AGV-1, G-2, PCC-1 and W1 was extracted from 200 mg-size samples using the purification method described below and summarized in Table 3, and the eluted matrix was subsequently doped with 500 ng W of known isotope composition (NIST SRM 3163). This allowed testing the W separation procedure in natural samples and checking possible matrix effects.

2.2 – Sample preparation and digestion

A variety of terrestrial rock standards have been analyzed in the frame of the present study, including andesites AGV-1 and AGV-2, basalts BE-N and BCR-1, diabase W1, granite G2, and peridotite PCC-1. Our new procedure was also applied to extraterrestrial materials: an ordinary chondrite (Dhajala, H3.8), a carbonaceous chondrite (Allende, CV3), and an iron meteorite (Gibeon, IVA).

Sample surfaces were stripped off using a tungsten-free diamond-coated stainless steel tool to remove any potential contamination. Samples were then crushed in a corundum mortar and subsequently dissolved in 15 mL Teflon Savillex© vials at 120°C on a hotplate during 5 to 10 days. Following the procedure developed by Quitté *et al.*[20], silicate-rich samples were

digested in a 6 mol.L^{-1} HCl - 27 mol.L^{-1} HF - 16 mol.L^{-1} HNO_3 mixture (proportions of 2:2:0.1 in volume, with a typical total volume of 10mL for 1 gram of sample). Metal-rich samples were digested in 6 mol.L^{-1} HCl - 27 mol.L^{-1} HF - 16 mol.L^{-1} HNO_3 (0.1:2:2 in volume) after dissolution of the outer part as detailed in Quitté *et al.*[20] to discard any potential contamination.

After digestion, the samples were evaporated to dryness and taken up twice in 6 mol.L^{-1} HCl. If some Ca- and Mg-fluorides still remained after this step, a few droplets (depending on the Ca and Mg concentration of the sample[20]) of a saturated H_3BO_3 solution were added to ensure a complete dissolution of the fluorides that may scavenge W by co-precipitation.

At this stage, a 5 vol.% aliquot was saved for further concentration analyses. As eluents used for the chromatography include HF, insoluble fluorides must be removed before the ion-exchange procedure to avoid precipitation on the column and plugging of the pores. After evaporation of the main fraction, 1 mol.L^{-1} HF (10mL per gram sample) was added to take up the residue and convert chlorides to fluorides. After drying down, 1 mol.L^{-1} HF was added a second time to ensure complete precipitation of fluorides. As we seek a quantitative recovery of W and as some W (and other HFSE – High Field Strength Elements) co-precipitates with fluorides[32,33], the latter have to be carefully rinsed with MilliQ H_2O, then re-dissolved in HCl and re-precipitated using HF. The procedure has to be repeated several times to get sure that no W remains trapped. In detail, the initial sample solution containing the fluorides was centrifuged (10 minutes at 5000 rpm) and the supernatant, containing most of the W, was saved. The fluoride precipitate was rinsed with H_2O and after centrifugation the second supernatant was added to the first one and the combined solution evaporated to dryness. The residue was then completely dissolved in an excess of 6 mol.L^{-1} HCl. This solution was evaporated to dryness before taking it up in 1 mol.L^{-1} HF to precipitate the fluorides again. A test performed using 1g of W-free Ca-Mg-fluorides precipitated from a Hawaii basalt and

doped with 200 ng of Alfa Aesar© W standard showed that the whole procedure has to be repeated at least twice. Indeed, the W content of fluorides resulting from the processing of the Hawaii basalt sample after 1 to 3 repetitions of the sequence described above decreased below detection limit after the second iteration (Figure 1). After 2 to 3 cycles of fluoride extraction, the combined supernatants were evaporated to dryness. No Ca and Mg remained in solution after this step, and all the W has been extracted from the precipitated fluorides. As 100% W is recovered at this stage, any mass-dependent effect on W caused by HFSE capture by CaF_2 and MgF_2 can be ruled out.

3 - Anion-Exchange Chromatography

The NIST SRM 3163 standard was processed twice using the procedure described by Irisawa and Hirata[31]. The yield was however 10 to 30% lower than expected and some mass-dependent fractionations were observed, induced by the chemical separation: the processed standard yielded a non-zero and non-reproducible isotope composition relative to the unprocessed standard. Besides, some W might be lost during sample decomposition due to its co-precipitation with the Ca- and Mg-fluorides, which may affect the W isotope composition. Indeed, the reaction forming WF_6 from WO_4^{2-} and the co-precipitation of WF_6 with $(Ca,Mg)F_2$ may induce isotope fractionation. We therefore set up an alternative method for separating and analyzing W stable isotopes in a wide variety of geological samples. This method relies on the properties of W in solution, which easily forms complexes with HF and H_2O_2.

The major interferences on W masses during MC-ICPMS analysis (Table 2) are Hf and Os (isobaric), Ta and Re (hydrides) and rare earth elements or REE (Ce, Nd, Sm, Eu, Gd, Dy, Ho, Er, Tm, Yb) which may form complex ions like argides (ArX^+), oxides (XO^+), dioxides

(XO_2^+), nitrides (XN^+) or fluorides (XF^+). Hence all these elements have to be carefully separated from W fraction during chromatography.

At least 20 ng W are required for a MC-ICPMS analysis and some samples are W-poor with concentrations down to 10 ppb. In this case, up to 2 g of sample have to be processed, hence large columns were used. The whole procedure may easily be scaled down for smaller samples, or if a purification step is needed.

After sample digestion and fluoride extraction, 10 mL of 1 $mol.L^{-1}$ HF were added to the residue and heated at 100°C on a hotplate overnight. The solution was then diluted by adding 6 mL of H_2O and 0.6 mL of 10% H_2O_2, and loaded onto a column filled with 10mL Bio-Rad AG1-X8 anionic resin (200-400 mesh, chloride form) previously cleaned and equilibrated with 2 $mol.L^{-1}$ HF - 4 $mol.L^{-1}$ HCl. The elution procedure is adapted from the procedure by Quitté *et al.*[20] and is summarized in Table 3. Many matrix elements are not retained on the resin and start eluting immediately. The remaining matrix as well as REE are then washed out with 70 mL 1 $mol.L^{-1}$ HCl - 2% H_2O_2. Tungsten is finally recovered in 60 mL 4 $mol.L^{-1}$ HNO_3 - 0.5 $mol.L^{-1}$ HF. This mixture was preferred to 4 $mol.L^{-1}$ HCl-2 $mol.L^{-1}$ HF to ensure the complete elution of W in the smallest possible volume. The analysis of the W cut revealed that only minor amounts of Mo were present, together with traces of Cd, Cr and Zn. No or minor traces of Os were found in the W fraction at this stage. Indeeed, a long (36-72h) and low-T evaporation of the recovered W fraction enabled to ensure the volatilization of this element. Mo/W ratios were always lower than 10^{-3}, so that the effect of Mo^{2+} on masses 184 and 186 was negligible, as demonstrated by Qin *et al.*[12]. REE, Ta, Hf and Re were completely absent from the W cut. The yield of our new procedure is 99.8 ± 1.2 % for W, with typical blanks of 50-100 pg W.

4 - Mass spectrometry

4.1 – Protocol

Isotope measurements have been performed at LGL-TPE, ENS de Lyon, using a Thermo Scientific© *Neptune Plus* instrument equipped with a Jet sampler cone and a X skimmer cone, which reduce odd/even isotope separation, improve sensitivity and reduce mass bias[34]. The instrument was connected to a *Cetac* Aridus desolvating system. Its sensitivity represents an asset for the study of W stable isotopes, as it limits the amount of rare material like meteorites required for one analysis while enabling a high precision determination of isotope ratios.

In order to ensure the stability of W in the analyzed solution, residues obtained after chromatography were taken up in a HNO_3 solution containing traces of HF (typically 0.05N). A run consisted of 2 blocks of 30 to 40 measurements. The typical sensitivity was 300-400 volts/ppm (amplifier resistor: 10^{11} ohm). Samples were analyzed 2 to 5 times at a concentration of 10 to 20 ppb using the standard-sample bracketing technique. As noticed by Qin *et al.*[35], a difference in relative concentrations between the standard and the sample may induce artifacts on the W isotope measurements. In the present study, W concentrations of the samples were adjusted within 5 % to the standard concentration, ensuring the artifact fractionation – if any – remained lower than 0.01 ‰.

The mass dispersion of the *Neptune Plus* MC-ICPMS permits to measure simultaneously the four major isotopes of tungsten (182, 183, 184, 186), two isotopes of the internal standard Hf (178, 179 - see next paragraph), as well as one isotope of Os (188) to correct the potential isobaric interferences on masses 184 and 186. The abundances of ^{184}Os and ^{186}Os are inferred using the canonical ratios: $^{184}Os/^{188}Os = 0.00149$ and $^{186}Os/^{188}Os = 0.11975$ [36]. The cup configuration is given in Table 4.

4.2 – Correction of the instrumental mass bias

The W isotope composition measured in meteorites results from several distinct contributions: the abundance of radiogenic ^{182}W (decay product of ^{182}Hf) is a function of the age of the

sample, while nucleosynthetic and cosmogenic effects also modify the W isotope ratios in a mass independent way[4,15,37,38]. Superimposed to these isotope anomalies are the mass dependent fractionations of W stable isotopes. Our new protocol was developed with the aim of studying at the same time stable isotope fractionation, nucleosynthetic anomalies and radioactive decay of ^{182}Hf (via the determination of ^{182}W abundance). The goal was therefore to get accurate determination of both stable isotope fractionation and mass independent anomalies. In this context, the use of a double-spike was excluded, and the instrumental mass bias was corrected for using an internal standard. Two elements were potential candidates: hafnium (Hf), and rhenium (Re) already used by Irisawa and Hirata[31]. Two series of a NIST SRM 3163 standard solution doped with either Hf or Re were measured on the same day in the frame of the present work to compare both approaches. The measurements performed using Hf as an internal standard display an external reproducibility of 0.04‰ for the ^{183}W/^{184}W isotope ratio whereas those with Re-doping have a reproducibility of 0.09‰ (Figure 2A). The Hf-doping was therefore selected, using a 1000 ppm Hf Alfa Aesar standard solution. The ^{180}W isotope cannot be measured due to the Hf isobaric interference: a precise interference correction is not achievable because of the relative abundances of both elements (Hf and W) on mass 180. ^{180}W is indeed the least abundant W isotope (0.13%) whereas the abundance of ^{180}Hf is 35.1 %. It is of note that the Hf-doping avoids the contribution of Re-hydride on mass 186.

The instrument generally induces a time dependent mass bias ascribed to instabilities in the nebulization chamber, matrix effects, and small variations of the gas flow conditions in the Aridus. Long-term variations of the instrumental mass bias were corrected for using the standard-sample bracketing technique (measurements of a standard solution are interspersed with analyses of samples), and run-to-run variations with Hf-doping. The mass bias β_{Hf} is estimated using the ^{178}Hf/^{179}Hf ratio:

$$\beta_{Hf} = \frac{\ln\left(\frac{\left(\frac{^{178}Hf}{^{179}Hf}\right)_{true}}{\left(\frac{^{178}Hf}{^{179}Hf}\right)_{measured}}\right)}{\ln\left(\frac{177.94371}{178.94583}\right)}$$

where $\left(\frac{^{178}Hf}{^{179}Hf}\right) = 2.00287$ [36].

The W isotope ratios are then corrected using a mass fractionation exponential law:

$$\left(\frac{^{i}W}{^{j}W}\right)_{corrected} = \left(\frac{^{i}W}{^{j}W}\right)_{measured} \left(\frac{i}{j}\right)^{\beta_{Hf}}$$

where ^{i}W and ^{j}W are two distinct W isotopes of respective masses *i* and *j*.

The amount of Hf added for doping is adjusted so as both standards and samples finally have the same Hf concentration. The accuracy and precision of the measurements were similar for Hf/W ratios of 0.5 to 1, as long as the Hf concentration enabled the Hf isotope composition to be measured with enough accuracy. As we aimed at analyzing small quantities of material including W-poor meteorites, standards and samples were measured at low W concentration. Consequently, Hf was added to achieve a Hf/W ratio of 1 to improve the precision of the correction.

Once corrected for the instrumental mass bias, W isotope ratios are expressed relative to the NIST SRM 3163 standard. As the ε notation is commonly used for the mass independent fractionation of tungsten isotopes, and contrarily to what has been proposed by Irisawa and Hirata[31], we suggest to use the common δ notation (per mil variations) to report mass dependent fractionations of W stable isotopes, even if the observed variations are often below 1 δ:

$$\delta(^{i}W/^{184}W) = 1000.\left(\frac{\left(\frac{^{i}W}{^{184}W}\right)^{spl}}{\left(\frac{^{i}W}{^{184}W}\right)^{std}} - 1\right)$$

$\left(\frac{^{i}W}{^{184}W}\right)^{spl}$ is the mass bias corrected isotope ratio of the sample and $\left(\frac{^{i}W}{^{184}W}\right)^{std}$ is the average value of the two bracketing standards. Analytical errors on the bracketing standards are not propagated into the δ value of the samples.

5 - Results and discussion

5.1. Isotope fractionation on the ion exchange resin and matrix effects

Figure 3 presents the elution curve and the total amount of W recovered (Figure 3A), along with the isotope composition of each 10 mL subfraction (Figure 3B). This graph allows recalculating the isotope composition of the recovered W fraction for yields lower than 100 % (Figure 3C). The NIST SRM 3163 standard fractionates on the column, the light isotopes going faster than the heavy ones. If only 80% of the total W is recovered, the procedure induces a systematic isotope fractionation of ≈0.05‰, comparable to the precision achieved on isotope measurements. A quantitative recovery of W is therefore required for studying stable isotope fractionation, which is the case of the chromatography procedure described above. The NIST SRM 3163 W standard solution processed through our protocol shows no evidence of procedure-induced isotope fractionation within error, as expected from a quantitative yield (Figure 4).

Matrix effects were checked by doping natural matrices with W standard after removing the naturally occurring W of the sample. The sample doped with the standard was processed again through the full chemical separation procedure and analyzed. Results for doped matrices are presented in Figure 4. All samples display the same isotope composition as the NIST SRM 3163 W standard within uncertainty, with a typical standard deviation (2SD, n = 3-4) better than 0.05 $\delta.amu^{-1}$, except for sample AGV-1-NIST that presents a larger error bar. Hence, our procedure does not induce any isotope fractionation related to matrix effects.

Additionally, the use of a Jet-X cones interface has previously been reported as generating unpredictable effects such as mass independent fractionation of ^{180}W [39]. In the present study, we did not observe any noticeable effect for the mass-dependent fractionation of W stable isotopes.

5.2. Reproducibility of the measurements

The external reproducibility (2SD) achieved for 20-30 replicates of W standard NIST SRM 3163 measured over a day at a concentration of 20 ppb (and interspersed with samples) is better than 0.09 δ or 90 ppm per amu for $^{182}W/^{184}W$, 0.07 δ or 70 ppm per amu for $^{183}W/^{184}W$, and 0.17 δ or 170 ppm per amu for $^{186}W/^{184}W$. The typical internal reproducibility for one measurement (2SD), be it for the standard or a sample, is 60 ppm, 50 ppm, and 140 ppm per amu for $^{182}W/^{184}W$, $^{183}W/^{184}W$, and $^{186}W/^{184}W$ respectively. Figure 2B shows a long-term reproducibility (2SD) of 80ppm for the $^{183}W/^{184}W$ ratio obtained for the standard over several sessions (2 months period), comparable to the one-day reproducibility.

5.3 – The case of ^{183}W

Recently, mass-independent anomalies were reported on ^{183}W for standards processed through a tungsten separation procedure[15]. According to the authors, these anomalies are related to a mass-independent fractionation between odd and even isotopes during sample preparation, W purification or re-dissolution of the purified W fraction. In the present piece of work, matrices doped with the NIST SRM 3163 W standard do not present either mass-dependent fractionation or any mass-independent effect. The anomalies observed in previous studies are potentially explained by the formation of small amounts of hydrides in the plasma during analysis. For the generation of a proportion p of W hydrides, we modeled the measured abundance on each mass with the following approximation:

$$[a_{18i}]_h = (1-p)[a_{18i}]_0 + p[a_{18i-1}]_0$$

Here, $[a_{18i}]_h$ represents the measured abundance on mass 18i (i=0, 2, 3, 4 or 6) and is defined as follows: $[a_{18i}]_h = [^{18i}W^+] - [^{18i}WH^+] + [^{18i-1}WH^+]$. $[a_{18i}]_0$ and $[a_{18i-1}]_0$ correspond to the theoretical abundance of each isotope when it exists (else 0).

After internal normalization to $^{186}W/^{183}W = 1.985935$, we calculated the deviation relative to a standard unaffected by hydride generation. This deviation is expressed in ε unit:

$$\varepsilon(^iW/^{184}W) = 10\,000.\left(\frac{\left(\frac{^iW}{^{184}W}\right)^{spl}}{\left(\frac{^iW}{^{184}W}\right)^{std}} - 1\right)$$

The line in Figure 5 represents the effect of a difference between standards and samples in terms of the proportion of W hydrides generated. An increase of 10ppm in the WH^+/W^+ ratio induces a shift of -0.171 ε of the $^{182}W/^{184}W$ ratio and of +0.076 ε of the $^{183}W/^{184}W$ ratio.

The W isotope data for NIST SRM 129c from Kruijer *et al.*[15] plot along the calculated line for hydrides generation. Thus, a small difference of 10-15 ppm of hydrides between standards and samples can be responsible for the observed mass independent anomalies (Figure 5). This could be an alternative explanation to the one proposed by Kruijer et al.[15] who pointed out problems of W loss during re-dissolution of the samples in Savillex beakers.

5.4 – Comparison with literature data

In the following, data are presented as variations of the isotopic composition per mass unit $\delta(\,^iW/^{184}W)/\Delta M$ (amu^{-1}):

$$\frac{\delta(\,^iW/^{184}W)}{\Delta M} = \frac{\delta(\,^iW/^{184}W)}{i-184}$$

Tungsten stable isotopes data are scarce in the literature. Irisawa[31,40] analyzed some terrestrial and meteoritic materials, among them the Gibeon IVA iron meteorite. To compare with our data set, we recalculated 2SD uncertainties from this previous study as Irisawa reported analytical errors as SE. Our data for Gibeon agree within uncertainty with those of Irisawa

(Figure 6), even if a small enrichment in heavy isotopes is now resolvable from the standard value. The small apparent shift between the average value for Gibeon in both sets of data might be due to an incomplete recovery of the tungsten fraction in the previous study, as presented in Figure 3: if the elution tail is not fully recovered, the measured isotope signature is indeed too light.

5.5 – Natural samples

Terrestrial volcanic and ultrabasic rock standards (AGV-1, AGV-2, BCR-1, BE-N, G2, PCC-1 and W1) as well as extraterrestrial materials (Allende, Dhajala and Gibeon meteorites) have been analyzed. Results are presented in Table 5. On Figure 7A, data for terrestrial samples plot on mass dependent isotope fractionation lines, but this is not the case for extraterrestrial samples (Figure 7B). For the latter, the abundance of radiogenic ^{182}W depends on the radioactive decay of ^{182}Hf, hence the $\delta^{182}W/^{184}W$ may be lower or higher than expected for a pure mass dependent fractionation. Besides, nucleosynthetic anomalies in meteorites may also modify the isotope pattern for $\delta^{183}W/^{184}W$ and $\delta^{186}W/^{184}W$. Such anomalies have not been corrected here, and may explain that the fractionation patterns do not intercept the *x*-axis at mass 183 in figure 7B. Small-uncorrected nucleosynthetic anomalies may also explain that uncertainties (2SD) calculated for extraterrestrial samples are somewhat higher than for terrestrial samples. In a $\delta^{183}W/^{184}W$ vs. $\delta^{186}W/^{184}W$ diagram (i.e. without considering ^{182}W), all natural samples – including meteorites – plot on a mass dependent fractionation line (Figure 8). As shown on Figure 9, replicate measurements perfectly agree with each other. This figure also demonstrates that some W isotope variability exists between natural samples: the mass-dependent fractionations observed in the terrestrial samples vary from -0.05 to +0.37 $\delta.amu^{-1}$. Peridotites present the lightest signature in average (-0.05 ± 0.10 $\delta.amu^{-1}$); the basaltic samples (BE-N, BCR-1, W1) all show a very homogeneous signature ranging from +0.09 to +0.14 $\delta.amu^{-1}$ (average: +0.11 ± 0.06 $\delta.amu^{-1}$). Andesitic rocks AGV-1 and AGV-2

display the heaviest signatures (+0.23 and +0.36 $\delta.amu^{-1}$) while granite G2 presents a lighter signature (-0.02 ± 0.06 $\delta.amu^{-1}$) undistinguishable from the NIST SRM 3163 standard. This isotope variability opens a new field of investigations and confirms the potential of W stable isotope fractionation to trace and apprehend geological processes.

Conclusions

A new method has been set up to analyze W stable isotopes. This protocol, based on a one-step anion-exchange chromatography, is suitable for a large variety of geological matrices. The procedure yield is 99.8 ± 1.2 %. The NIST SRM 3163 standard solution (with or without a rock matrix) processed through the ion-exchange resin showed no mass-dependent isotope fractionation within error. Hafnium, more specifically the $^{178}Hf/^{179}Hf$ ratio, was used as an internal standard to correct the instrumental mass bias. Alternatively, the $^{185}Re/^{187}Re$ ratio may also be used even if the uncertainties on the normalized values are then slightly larger. Tungsten stable isotope measurements performed with the last generation Neptune *Plus* MC-ICPMS equipped with Jet cones are 10 to 20 times more sensitive than those reported in previous studies with other instruments.

Our new method was applied to terrestrial and extraterrestrial samples: they present various and distinct stable isotope signatures. Even if the measured W mass dependent isotope fractionation is in most cases <0.5 $\delta.amu^{-1}$, the variations are clearly resolvable from the standard value within uncertainties. Thus, the present piece of work confirms the potential of W stable isotopes to trace geological processes.

Acknowledgements

We are grateful to P. Télouk for maintaining the ICPMS instruments running well. We also acknowledge the MNHN (Paris) for providing meteorite samples. Last but not least, we thank

the two anonymous reviewers for their advices and comments that helped improving the manuscript.

This work was supported by the French National Program of Planetology (PNP).

References

1. C. Burkhardt, T. Kleine, B. Bourdon, H. Palme, J. Zipfel, J. M. Friedrich, and D. S. Ebel, *Geochim. Cosmochim. Acta*, 2008, **72**, 6177–6197.

2. T. Kleine, K. Mezger, H. Palme, E. Scherer, and C. Münker, *Geochim. Cosmochim. Acta*, 2005, **69**, 5805–5818.

3. A. Markowski, Ph.D. thesis, ETH Zürich, 2006.

4. A. Markowski, I. Leya, G. Quitté, K. Ammon, A. N. Halliday, and R. Wieler, *Earth Planet. Sci. Lett.*, 2006, **250**, 104–115.

5. A. Markowski, G. Quitté, T. Kleine, A. Halliday, M. Bizzarro, and A. Irving, *Earth Planet. Sci. Lett.*, 2007, **262**, 214–229.

6. A. Markowski, G. Quitté, A. Halliday, and T. Kleine, *Earth Planet. Sci. Lett.*, 2006, **242**, 1–15.

7. G. Quitté and J.-L. Birck, *Earth Planet. Sci. Lett.*, 2004, **219**, 201–207.

8. T. Schulz, C. Münker, K. Mezger, and H. Palme, *Geochim. Cosmochim. Acta*, 2010, **74**, 1706–1718.

9. T. Schulz, C. Münker, H. Palme, and K. Mezger, *Earth Planet. Sci. Lett.*, 2009, **280**, 185–193.

10. C. Burkhardt, T. Kleine, N. Dauphas, and R. Wieler, *Astrophys. J.*, 2012, **753**, L6.

11. K. Irisawa, Q.-Z. Yin, and T. Hirata, *Geochem. J.*, 2009, **43**, 395–402.

12. L. Qin, N. Dauphas, M. Wadhwa, A. Markowski, R. Gallino, P. E. Janney, and C. Bouman, *Astrophys. J.*, 2008, **674**, 1234–1241.

13. L. Qin, N. Dauphas, M. Wadhwa, J. Masarik, and P. E. Janney, *Earth Planet. Sci. Lett.*, 2008, **273**, 94–104.

14. A. Scherstén, T. Elliott, C. Hawkesworth, S. Russell, and J. Masarik, *Earth Planet. Sci. Lett.*, 2006, **241**, 530–542.

15. T. S. Kruijer, P. Sprung, T. Kleine, I. Leya, C. Burkhardt, and R. Wieler, *Geochim. Cosmochim. Acta*, 2012, **99**, 287–304.

16. T. Kleine, M. Touboul, J. A. Van Orman, B. Bourdon, C. Maden, K. Mezger, and A. N. Halliday, *Earth Planet. Sci. Lett.*, 2008, **270**, 106–118.

17. G. Quitté, J. Birck, and C. J. Allègre, *Earth Planet. Sci. Lett.*, 2000, **184**, 83–94.

18. D.-C. Lee, A. N. Halliday, S. J. Singletary, and T. L. Grove, *Earth Planet. Sci. Lett.*, 2009, **288**, 611–618.

19. M. Touboul, T. Kleine, B. Bourdon, J. A. Van Orman, C. Maden, and J. Zipfel, *Earth Planet. Sci. Lett.*, 2009, **284**, 168–178.

20. G. Quitté, J.-L. Birck, F. Capmas, and C. J. Allègre, *Geostand. Geoanalytical Res.*, 2002, **26**, 149–160.

21. M. Touboul and R. J. Walker, *Int. J. Mass Spectrom.*, 2011, **309**, 109–117.

22. W. Abouchami, S. J. G. Galer, T. J. Horner, M. Rehkämper, F. Wombacher, Z. Xue, M. Lambelet, M. Gault-Ringold, C. H. Stirling, M. Schönbächler, A. E. Shiel, D. Weis, and P. F. Holdship, *Geostand. Geoanalytical Res.*, 2013, **37**, 5–17.

23. F. Wombacher, M. Rehkämper, K. Mezger, C. Münker, and A. Bischoff, *Goldschmidt Conf. Abstr.*, 2002.

24. F. Wombacher, M. Rehkämper, K. Mezger, A. Bischoff, and C. Münker, *Geochim. Cosmochim. Acta*, 2008, **72**, 646–667.

25. F. Wombacher, M. Rehkämper, K. Mezger, and C. Münker, *Geochim. Cosmochim. Acta*, 2003, **67**, 4639–4654.

26. C. Burkhardt, R. C. Hin, T. Kleine, and B. Bourdon, *Earth Planet. Sci. Lett.*, 2014, **391**, 201–211.

27. S. G. Nielsen, M. Rehkämper, D. Porcelli, P. Andersson, A. N. Halliday, P. W. Swarzenski, C. Latkoczy, and D. Günther, *Geochim. Cosmochim. Acta*, 2005, **69**, 2007–2019.

28. S. G. Nielsen, M. Goff, S. P. Hesselbo, H. C. Jenkyns, D. E. LaRowe, and C.-T. A. Lee, *Geochim. Cosmochim. Acta*, 2011, **75**, 6690–6704.

29. S. G. Nielsen, L. E. Wasylenki, M. Rehkämper, C. L. Peacock, Z. Xue, and E. M. Moon, *Geochim. Cosmochim. Acta*, 2013, **117**, 252–265.

30. M. Rehkämper, M. Frank, J. R. Hein, D. Porcelli, A. Halliday, J. Ingri, and V. Liebetrau, *Earth Planet. Sci. Lett.*, 2002, **197**, 65–81.

31. K. Irisawa and T. Hirata, *J. Anal. At. Spectrom.*, 2006, **21**, 1387.

32. A. Makishima and E. Nakamura, *Geostand. Geoanalytical Res.*, 1999, **23**, 137–148.

33. R. Tanaka, A. Makishima, H. Kitagawa, and E. Nakamura, *J. Anal. At. Spectrom.*, 2003, **18**, 1458.

34. N. Shirai and M. Humayun, *J. Anal. At. Spectrom.*, 2011, **26**, 1414.

35. L. Qin, N. Dauphas, P. E. Janney, and M. Wadhwa, *Anal. Chem.*, 2007, **79**, 3148–54.

36. K. J. R. Rosman and P. D. P. Taylor, *Pure Appl. Chem.*, 1998, **70**, 217–235.

37. I. Leya, H. Lange, S. Neumann, R. Wieler, and R. Michel, *Meteorit. Planet. Sci.*, 2000, **35**, 259–286.

38. N. Wittig, M. Humayun, A. D. Brandon, S. Huang, and I. Leya, *Earth Planet. Sci. Lett.*, 2013, **361**, 152–161.

39. T. Schulz, C. Münker, and S. T. M. Peters, *Earth Planet. Sci. Lett.*, 2013, **362**, 246–257.

40. K. Irisawa, Ph.D. thesis, Tokyo Institute of Technology, 2007.

Tables and Figures

Table 1: Blank values for the concentrated reagents used in this study. H_2O_2: Merck Suprapur commercial reagent; mineral acids: * distilled; ** bi-distilled.

Table 2: Isobars and main molecular interferences on W isotopes.

Table 3: Elution scheme for the quantitative recovery of W. The column is filled with 10 mL Biorad AG1-X8 (200-400 mesh) anion-exchange resin in chloride form.

Table 4: Cup configuration on the *Neptune Plus* MC-ICPMS for the analysis of W stable isotopes and correction of Os isobaric interferences. Hf was used as an internal standard to correct the instrumental mass bias (see text).

Table 5: W stable isotope data for terrestrial reference materials and meteorites. Results are internally normalized to $^{178}Hf/^{179}Hf$ = 2.00287 (Rosman and Taylor, 1998). AGV-1 and

AGV-2: andesite; G2: granite; PCC-1: peridotite; W1: diabase; BCR1 and BE-N: basalts. The column on the right displays the weighted mean of the measured $\delta.amu^{-1}$ relevant to the sample (i.e. we did not take the $^{182}W/^{184}W$ ratio into account for meteorite samples). 2SD of individual samples refer to two internal analytical errors; 2SD of the mean was calculated as the deviation about the mean. The error associated to the mean value of a population is calculated as 2SE.

Figure 1: Proportion of tungsten that remains trapped in the fluorides after each dissolution-precipitation and washing step. 200 ng of W and 1g of (Ca,Mg)-fluorides were used for these tests.

Figure 2: A - Comparison of the mean values and reproducibility of the standard, using Re-doping or Hf-doping to correct the instrumental mass bias. Grey fields correspond to two standard deviations (2SD) calculated on the measured values. Different standard solutions have been tested, as well as different procedures: (a_1) 20 ppb W + 20 ppb Re; (a_2) 20 ppb W + 20 ppb Re + sample bracketing; (b_1) 20 ppb W + 20 ppb Hf; (b_2) 20 ppb W + 20 ppb Hf + sample bracketing; (c_1) 10 ppb W + 10 ppb Hf; (c_2) 10 ppb W + 10 ppb Hf + sample bracketing. **B** - Long-term variability (April to June 2013) of the standard mass-dependent fractionation. The standards were interspersed with samples, which are not reported here. Error bars are within-run statistics (2SD) on the raw ratios.

Figure 3: Fractionation of W isotopes during ion-exchange. **A** – Fraction of W eluted as a function of the volume, both in the successive 10mL elution fractions (dashed line) and total fraction of eluted W (grey line). **B** – deviation of W stable isotope signature in each fraction relative to the unprocessed standard. **C** – deviation of the W stable isotope signature in the cumulative W fraction.

Figure 4: Check for matrix effects on W isotope fractionation (per mass unit) during the purification stage through anion-exchange resin AG1-X8 (200-400 mesh). In this diagram, AGV-1, PCC-1, G2 and W1 represent the rock matrices extracted from the corresponding rock standards, respectively andesite, peridotite, granite and diabase. After complete extraction of their natural W, the geological standard rock matrices were doped with 500 ng of NIST SRM 3163 W. * denotes the pure (i.e. without rock matrix) NIST SRM 3163 standard processed through the chromatography procedure as a sample. *n* represents the number of MC-ICPMS replicate measurements. In this diagram, the reported $\delta^{i}W/\Delta M$ is the average of the measured $\delta(^{182}W/^{184}W)$, $\delta(^{183}W/^{184}W)$ and $\delta(^{186}W/^{184}W)$ values divided by their respective mass differences (e.g. $\delta(^{182}W/^{184}W)/2$). Error bars correspond to 2SD uncertainties. All samples yield the same isotope composition as the pure standard solution, confirming the absence of any matrix effect.

Figure 5: Effects of the variability in hydrides formation between standards and samples during W mass spectrometry analysis (black line) compared to the data obtained by (Kruijer et al., 2012), and internally normalized to $^{186}W/^{183}W = 1.985935$ (noted 6/3). In this diagram, we model the formation of hydrides on a NIST SRM 3163 standard as follows: we supposed a hydride generation on each isotope proportionally to the abundance of the isotope. The length of the black arrow represents a 10 ppm hydride generation difference between sample and standard. See text for calculation details.

Figure 6: Comparison of the measured $\delta^{184}W/^{183}W$ for Gibeon (IVA iron meteorite) with data from the literature. Black dots are values from Irisawa (2007) in which 2SD errors were recalculated from the reported SE errors. Open squares are values obtained in the present study. Error bars are within-run statistics (2SD) on the raw ratios.

Figure 7: Measured $\delta^{18X}W$ (X=2, 3, or 6) reported as a function of the mass. For clarity, error bars were not reported on this figure but can be found in Table 5. **A** – Data for terrestrial samples (rock standards: andesite (AGV-1, AGV-2), basalt (BCR-1, BE-N), diabase (W1), granite (G-2) and peridotite (PCC-1)). **B** – Data for meteorite samples (ordinary chondrite: Dhajala (H3.8); carbonaceous chondrite: Allende (CV3); and iron meteorite: Gibeon (IVA)).

Figure 8: Mass-dependent fractionation of W isotopes in mafic and ultramafic rock samples. In a three isotopes diagram, the samples fall on the theoretical mass-dependent fractionation line (grey line). Symbols correspond to the weighted average and the propagated error (2SD). Symbols are the same as on Figure 7.

Figure 9: Mean values of the mass-dependent fractionation of W isotopes in terrestrial and extraterrestrial samples. Each sample has been measured 2 to 6 times. Replicates for Gibeon are presented in figure 6 ($\delta^{184}W/^{183}W$). Reported error bars correspond to two standard deviations from the mean value ($\delta.amu^{-1}$) for each measured sample. Larger symbols represent the mean of the measurements for each rock and their error bars correspond to 2SE (two standard errors) about the mean value $\delta.amu^{-1}$ for all the measured samples of the rock.

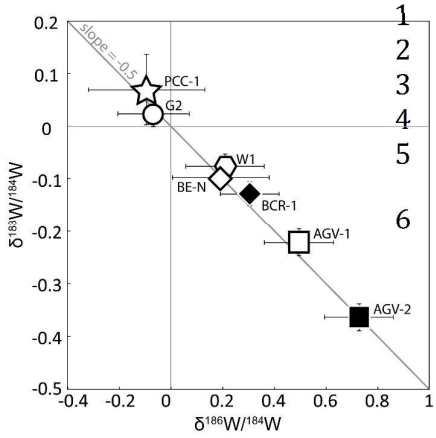

A new method for high precision measurements of W stable isotopes by MC-ICPMS enables to discriminate small mass-dependent fractionations, with applications in numerous fields of earth, planetary and environmental sciences.

Isotope (abundance)	^{180}W (0.12 %)	^{182}W (26.50 %)	^{183}W (14.31 %)	^{184}W (30.64 %)	^{186}W (28.43%)
Interferences:					
Isobaric	^{180}Hf ^{180}Ta			^{184}Os	^{186}Os
Argides	Not measured	^{40}Ar^{142}Ce^{+} ^{40}Ar^{142}Nd^{+} ^{36}Ar^{146}Nd^{+}	^{40}Ar^{143}Nd^{+} ^{36}Ar^{147}Nd^{+}	^{40}Ar^{144}Nd^{+} ^{40}Ar^{144}Sm^{+} ^{36}Ar^{148}Nd^{+} ^{36}Ar^{148}Sm^{+}	^{40}Ar^{146}Nd^{+} ^{36}Ar^{150}Nd^{+} ^{36}Ar^{150}Sm^{+}
Hydrides	-	^{181}TaH^{+}	^{182}WH^{+}	^{183}WH^{+}	^{185}ReH^{+}
Oxides	-	^{165}Ho^{17}O^{+} ^{166}Er^{16}O^{+}	^{167}Er^{16}O^{+} ^{166}Er^{17}O^{+}	^{167}Er^{17}O^{+} ^{168}Er^{16}O^{+}	^{169}Yb^{17}O^{+} ^{170}Tm^{16}O^{+}
Dioxides	-	^{149}Sm^{16}O^{17}O^{+} ^{150}Sm^{16}O^{16}O^{+} ^{150}Nd^{16}O^{16}O^{+}	^{150}Sm^{16}O^{17}O^{+} ^{150}Nd^{16}O^{17}O^{+} ^{151}Eu^{16}O^{16}O^{+}	^{151}Eu^{16}O^{17}O^{+} ^{152}Sm^{16}O^{16}O^{+}	^{153}Eu^{16}O^{17}O^{+} ^{154}Sm^{16}O^{16}O^{+} ^{154}Gd^{16}O^{16}O^{+}
Nitrides	-	^{168}Er^{14}N^{+}	^{169}Tm^{14}N^{+}	^{170}Er^{14}N^{+} ^{170}Yb^{14}N^{+}	^{172}Yb^{14}N^{+}
Fluorides	-	^{163}Dy^{19}F^{+}	^{164}Dy^{19}F^{+} ^{164}Er^{19}F^{+}	^{165}Ho^{19}F^{+}	^{167}Er^{19}F^{+}
Others	-	*Composed ions, Chlorides (Nd, Sm, Eu), Hydroxides (Ho, Er, Tm)*			

Table 2

Reagent	Concentration	W (pg/mL)
HF^{**}	26 $mol.L^{-1}$	3
HNO_3^{*}	15 $mol.L^{-1}$	0.8
HCl^{*}	10 $mol.L^{-1}$	0.07
H_2O_2	30 %	0.01
H_2O MilliQ	-	0.001

Table 1

Step	Acid	Volume	Eluted elements
Cleaning	2 mol.L^{-1} HF - 4 mol.L^{-1} HCl	40 mL	
The cleaning cycle is repeated a second time	H_2O	40 mL	
	4 mol.L^{-1} HNO_3 - 0.5 mol.L^{-1} HF	40 mL	
	H_2O	40 mL	
Resin equilibration	2 mol.L^{-1} HF - 4 mol.L^{-1} HCl	40 mL	
Sample introduction	0.6 mol.L^{-1} HF - 0.36% H_2O_2	16.6 mL	Major elements, Ba, Pb, Cr, Co, Ni, Cu, Zn, Rb, Sr, Ta, Re
Washing	1 mol.L^{-1} HCl - 2% H_2O_2	70 mL	REE, Ti, Al
W Elution	4 mol.L^{-1} HNO_3 - 0.5 mol.L^{-1} HF	60 mL	W (+Mo)

Table 3

Cup	L4	L3	L2	L1	C	H1	H2	H3	H4
Mass	178	179	-	182	183	184	186	188	-
Element	Hf	Hf	-	W	W	W + Os	W + Os	Os	-

Table 4

	$\delta^{182}W/^{184}W$	*2SD*	$\delta^{183}W/^{184}W$	*2SD*	$\delta^{186}W/^{184}W$	*2SD*	$\delta(2/4)$ (amu^{-1})	*2SD*	$\delta(3/4)$ (amu^{-1})	*2SD*	$\delta(6/4)$ (amu^{-1})	*2SD*	$\delta.amu^{-1}$	***2SD***
AGV-1	-0.48	*0.12*	-0.27	*0.05*	0.58	*0.29*	0.24	*0.06*	0.27	*0.05*	0.29	*0.15*	0.27	0.05
	-0.37	*0.13*	-0.18	*0.06*	0.44	*0.31*	0.19	*0.07*	0.18	*0.06*	0.22	*0.16*	0.20	0.04
	-0.44	*0.10*	-0.23	*0.07*	0.54	*0.28*	0.22	*0.05*	0.23	*0.07*	0.27	*0.14*	0.24	0.05
	-0.40	*0.14*	-0.19	*0.05*	0.46	*0.32*	0.20	*0.07*	0.19	*0.05*	0.23	*0.16*	0.21	0.04
	-0.50	*0.12*	-0.24	*0.06*	0.46	*0.30*	0.25	*0.06*	0.24	*0.06*	0.23	*0.15*	0.24	0.02
Mean													**0.23**	**0.02**
AGV-2	-0.75	*0.14*	-0.37	*0.06*	0.76	*0.31*	0.37	*0.07*	0.37	*0.06*	0.38	*0.16*	0.37	0.01
	-0.71	*0.12*	-0.38	*0.05*	0.66	*0.27*	0.36	*0.06*	0.38	*0.05*	0.33	*0.14*	0.36	0.05
	-0.66	*0.14*	-0.36	*0.05*	0.76	*0.26*	0.33	*0.07*	0.36	*0.05*	0.38	*0.13*	0.36	0.05
	-0.74	*0.08*	-0.38	*0.06*	0.70	*0.36*	0.37	*0.04*	0.38	*0.06*	0.35	*0.18*	0.37	0.03
	-0.62	*0.12*	-0.33	*0.07*	0.76	*0.32*	0.31	*0.06*	0.33	*0.07*	0.38	*0.16*	0.34	0.07
Mean													**0.36**	**0.01**
G2	-0.06	*0.10*	0.06	*0.06*	-0.06	*0.25*	0.03	*0.05*	-0.06	*0.06*	-0.03	*0.13*	-0.02	0.09
	-0.05	*0.12*	0.02	*0.05*	-0.11	*0.39*	0.02	*0.06*	-0.02	*0.05*	-0.06	*0.20*	-0.02	0.08
	0.00	*0.08*	0.01	*0.05*	-0.02	*0.34*	0.00	*0.04*	-0.01	*0.05*	-0.01	*0.17*	-0.01	0.01
	0.04	*0.14*	0.03	*0.06*	-0.06	*0.34*	-0.02	*0.07*	-0.03	*0.06*	-0.03	*0.17*	-0.03	0.01
	-0.06	*0.12*	0.00	*0.06*	-0.08	*0.28*	0.03	*0.06*	0.00	*0.06*	-0.04	*0.14*	0.00	0.07
Mean													**-0.02**	**0.01**
PCC-1	0.11	*0.18*	0.09	*0.10*	-0.02	*0.36*	-0.05	*0.09*	-0.09	*0.10*	-0.01	*0.18*	-0.05	0.08
	0.16	*0.20*	0.12	*0.12*	-0.22	*0.40*	-0.08	*0.10*	-0.12	*0.12*	-0.11	*0.20*	-0.10	0.04
	0.00	*0.16*	0.00	*0.14*	-0.04	*0.42*	0.00	*0.08*	0.00	*0.14*	-0.02	*0.21*	-0.01	0.02
Mean													**-0.05**	**0.03**
W1	-0.17	*0.14*	-0.04	*0.06*	0.32	*0.34*	0.08	*0.07*	0.04	*0.06*	0.16	*0.17*	0.09	0.12
	-0.16	*0.13*	-0.08	*0.04*	0.21	*0.35*	0.08	*0.07*	0.08	*0.04*	0.10	*0.18*	0.09	0.02
	-0.14	*0.12*	-0.09	*0.05*	0.20	*0.38*	0.07	*0.06*	0.09	*0.05*	0.10	*0.19*	0.09	0.03
	-0.16	*0.14*	-0.07	*0.07*	0.18	*0.30*	0.08	*0.07*	0.07	*0.07*	0.09	*0.15*	0.08	0.02
	-0.18	*0.16*	-0.10	*0.07*	0.14	*0.34*	0.09	*0.08*	0.10	*0.07*	0.07	*0.17*	0.09	0.03
Mean													**0.09**	**0.01**
BCR-1	-0.24	*0.12*	-0.12	*0.05*	0.31	*0.22*	0.12	*0.06*	0.12	*0.05*	0.16	*0.11*	0.13	0.05
	-0.24	*0.12*	-0.13	*0.04*	0.30	*0.27*	0.12	*0.06*	0.13	*0.04*	0.15	*0.14*	0.13	0.03
	-0.20	*0.10*	-0.10	*0.06*	0.24	*0.26*	0.10	*0.05*	0.10	*0.06*	0.12	*0.13*	0.11	0.02
	-0.32	*0.12*	-0.14	*0.05*	0.34	*0.28*	0.16	*0.06*	0.14	*0.05*	0.17	*0.14*	0.16	0.03
	-0.24	*0.14*	-0.15	*0.07*	0.34	*0.26*	0.12	*0.07*	0.15	*0.07*	0.17	*0.13*	0.15	0.05
Mean													**0.14**	**0.01**
BE-N	-0.18	*0.08*	-0.11	*0.03*	0.19	*0.45*	0.09	*0.04*	0.11	*0.03*	0.10	*0.23*	0.10	0.02
	-0.14	*0.06*	-0.09	*0.03*	0.26	*0.50*	0.07	*0.03*	0.09	*0.03*	0.13	*0.25*	0.10	0.06
	-0.20	*0.10*	-0.10	*0.02*	0.18	*0.38*	0.1	*0.05*	0.10	*0.02*	0.09	*0.19*	0.10	0.01
	-0.22	*0.08*	-0.10	*0.04*	0.18	*0.42*	0.11	*0.04*	0.10	*0.04*	0.09	*0.21*	0.10	0.02
	-0.14	*0.06*	-0.09	*0.04*	0.16	*0.38*	0.07	*0.03*	0.09	*0.04*	0.08	*0.19*	0.08	0.02
Mean													**0.09**	**0.01**
Allende	-0.82	*0.06*	-0.36	*0.02*	0.58	*0.29*	0.41	*0.03*	0.36	*0.02*	0.29	*0.14*	0.33	0.10
	-0.81	*0.05*	-0.35	*0.02*	0.55	*0.30*	0.40	*0.03*	0.35	*0.02*	0.28	*0.15*	0.32	0.10
	-0.81	*0.06*	-0.36	*0.03*	0.56	*0.26*	0.41	*0.03*	0.36	*0.03*	0.28	*0.13*	0.32	0.11
Mean													**0.32**	**0.03**
Dhajala	-0.51	*0.08*	-0.16	*0.03*	0.15	*0.36*	0.25	*0.04*	0.16	*0.03*	0.07	*0.18*	0.12	0.13
	-0.56	*0.08*	-0.19	*0.03*	0.21	*0.37*	0.28	*0.04*	0.19	*0.03*	0.10	*0.19*	0.15	0.13
Mean													**0.13**	**0.05**
Gibeon	-0.70	*0.08*	-0.20	*0.03*	0.51	*0.60*	0.35	*0.04*	0.20	*0.03*	0.25	*0.30*	0.23	0.07
	-0.73	*0.06*	-0.20	*0.04*	0.23	*0.37*	0.37	*0.03*	0.20	*0.04*	0.12	*0.19*	0.16	0.11
	-0.60	*0.07*	-0.13	*0.03*	0.36	*0.51*	0.30	*0.04*	0.13	*0.03*	0.18	*0.26*	0.16	0.07
	-0.61	*0.08*	-0.17	*0.04*	0.32	*0.42*	0.30	*0.04*	0.17	*0.04*	0.16	*0.21*	0.17	0.01
	-0.58	*0.09*	-0.12	*0.04*	0.33	*0.73*	0.29	*0.05*	0.12	*0.04*	0.16	*0.37*	0.14	0.06
	-0.53	*0.09*	-0.15	*0.06*	0.22	*0.75*	0.27	*0.05*	0.15	*0.06*	0.11	*0.38*	0.13	0.06
Mean													**0.16**	**0.02**

Table 5

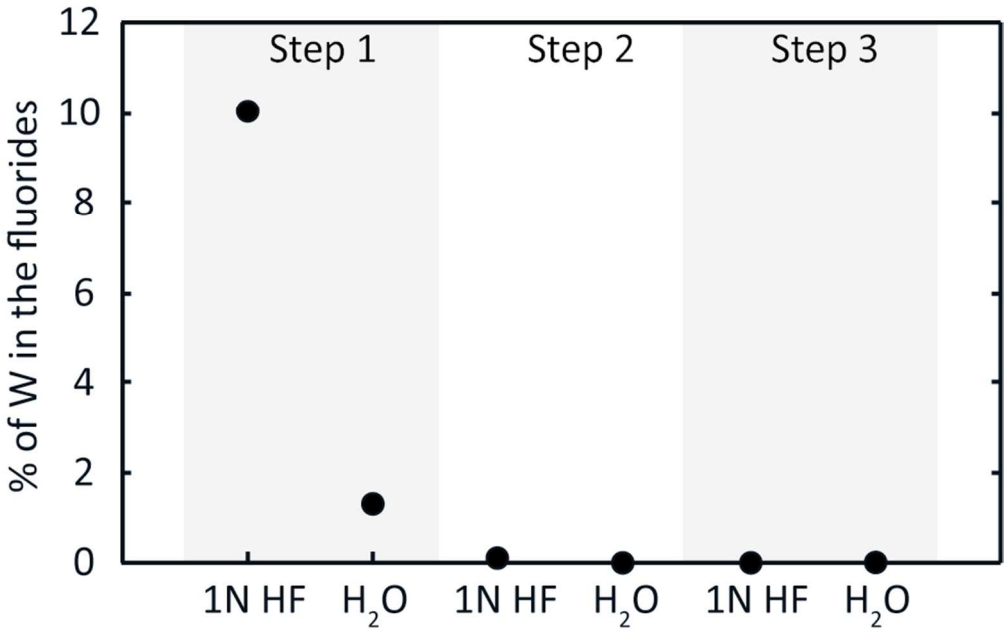

Figure 1
82x53mm (300 x 300 DPI)

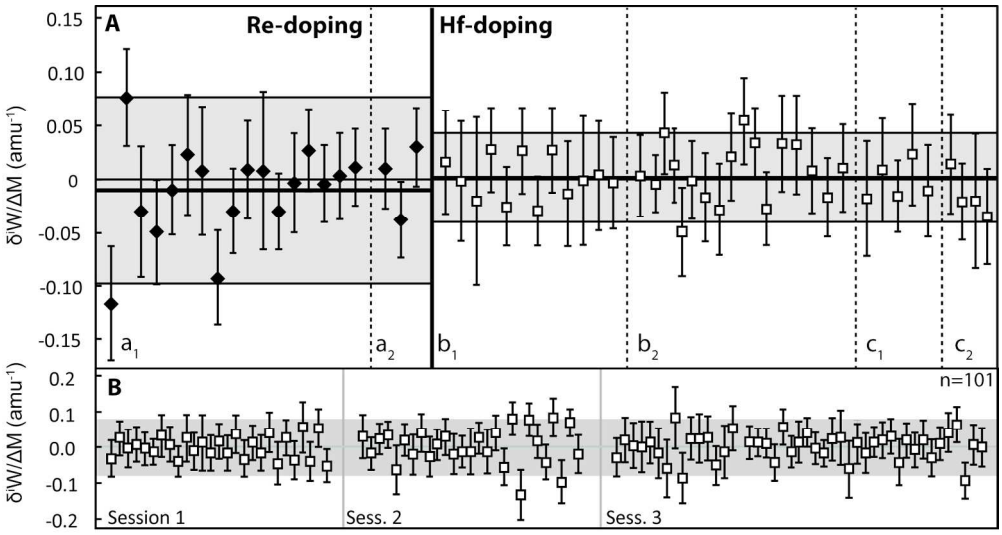

Figure 2
170x90mm (300 x 300 DPI)

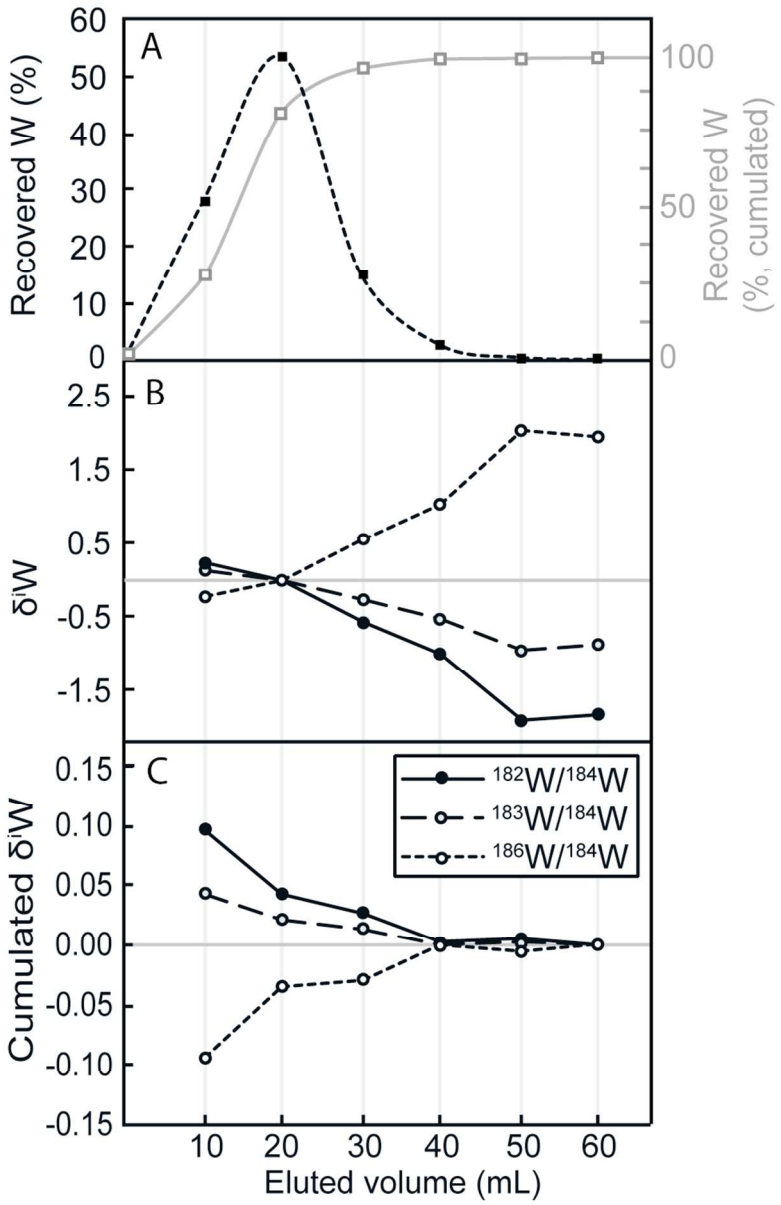

Figure 3
83x127mm (300 x 300 DPI)

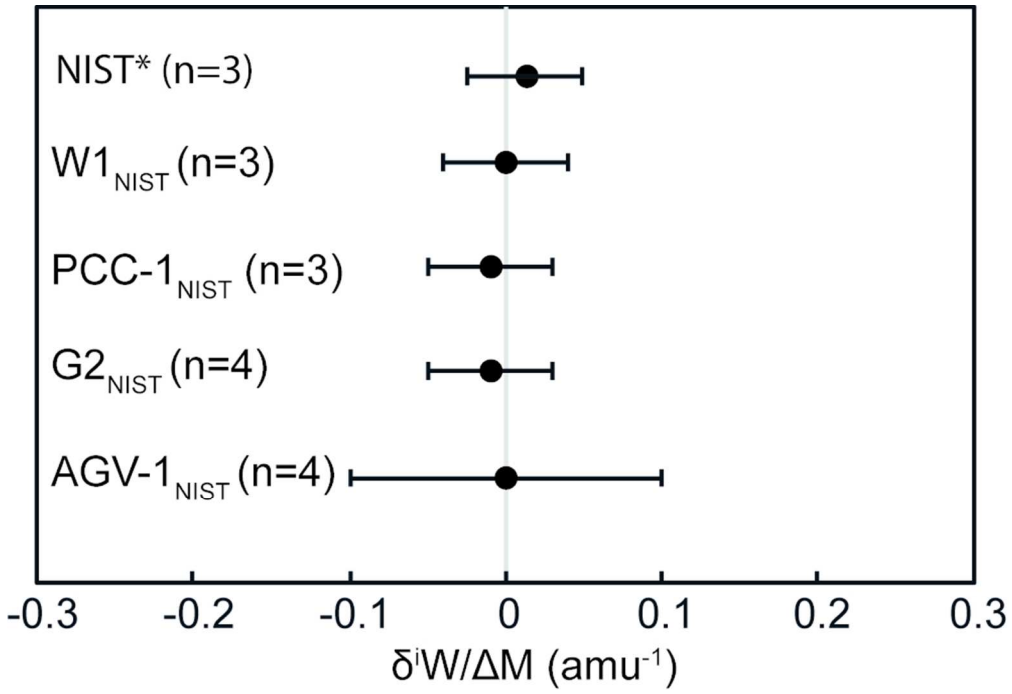

Figure 4
84x57mm (300 x 300 DPI)

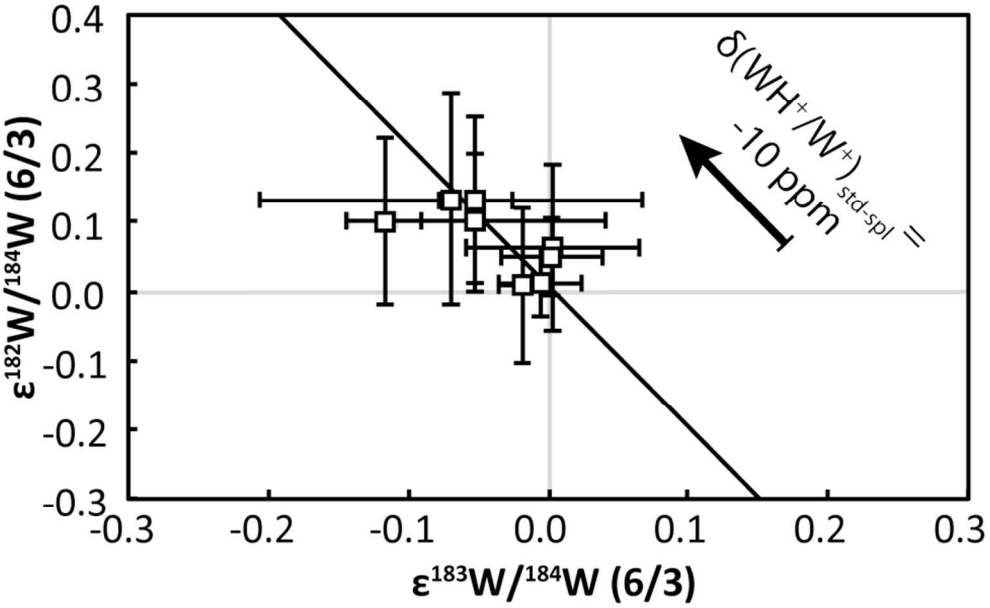

Figure 5
83x51mm (300 x 300 DPI)

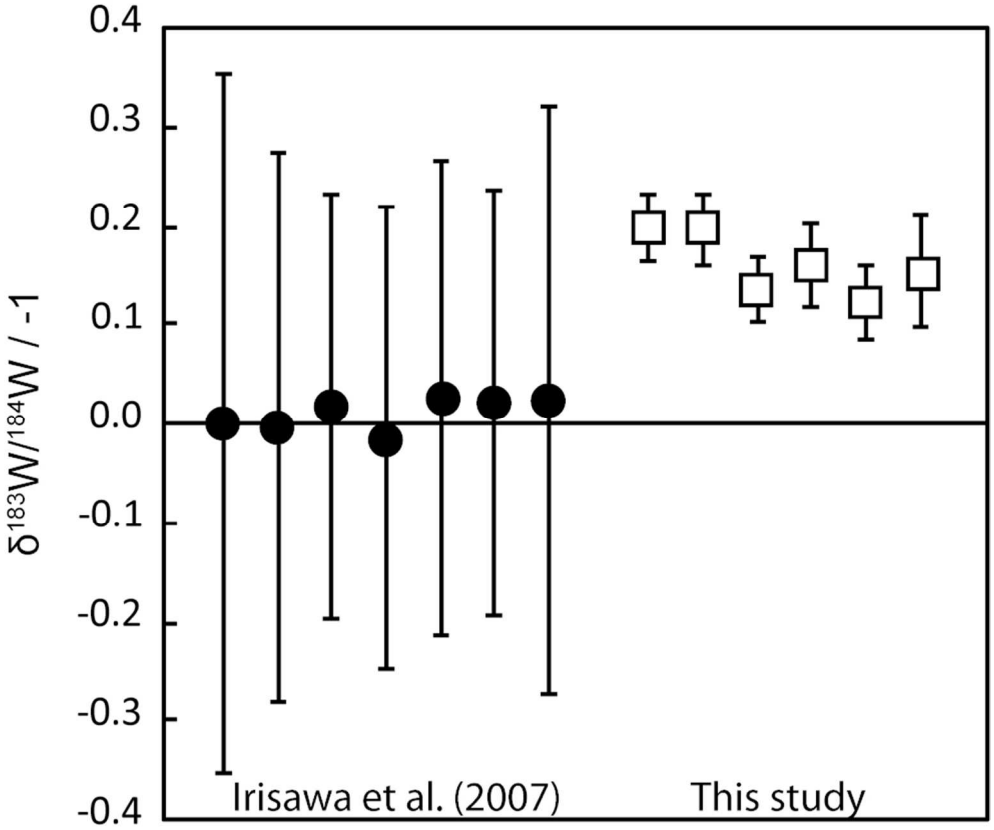

Figure 6
84x71mm (300 x 300 DPI)

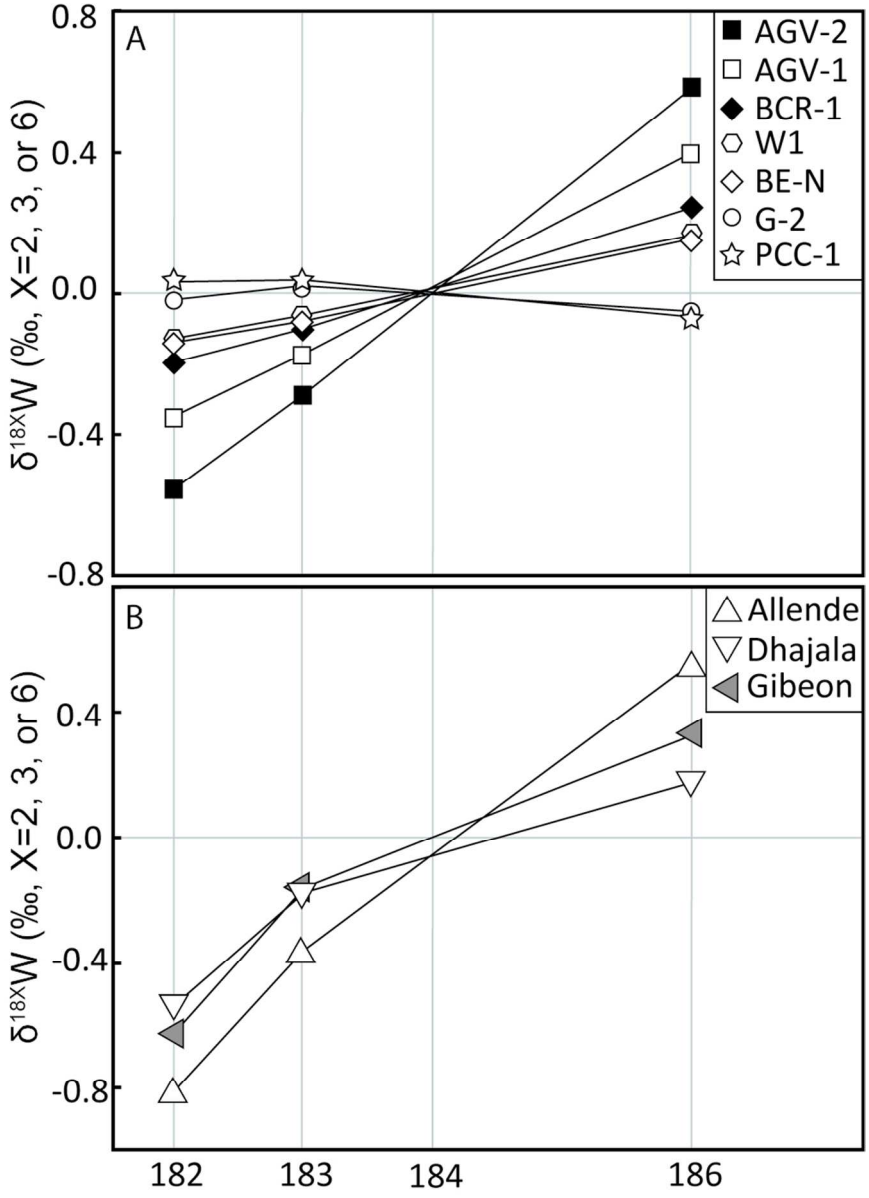

Figure 7
85x118mm (300 x 300 DPI)

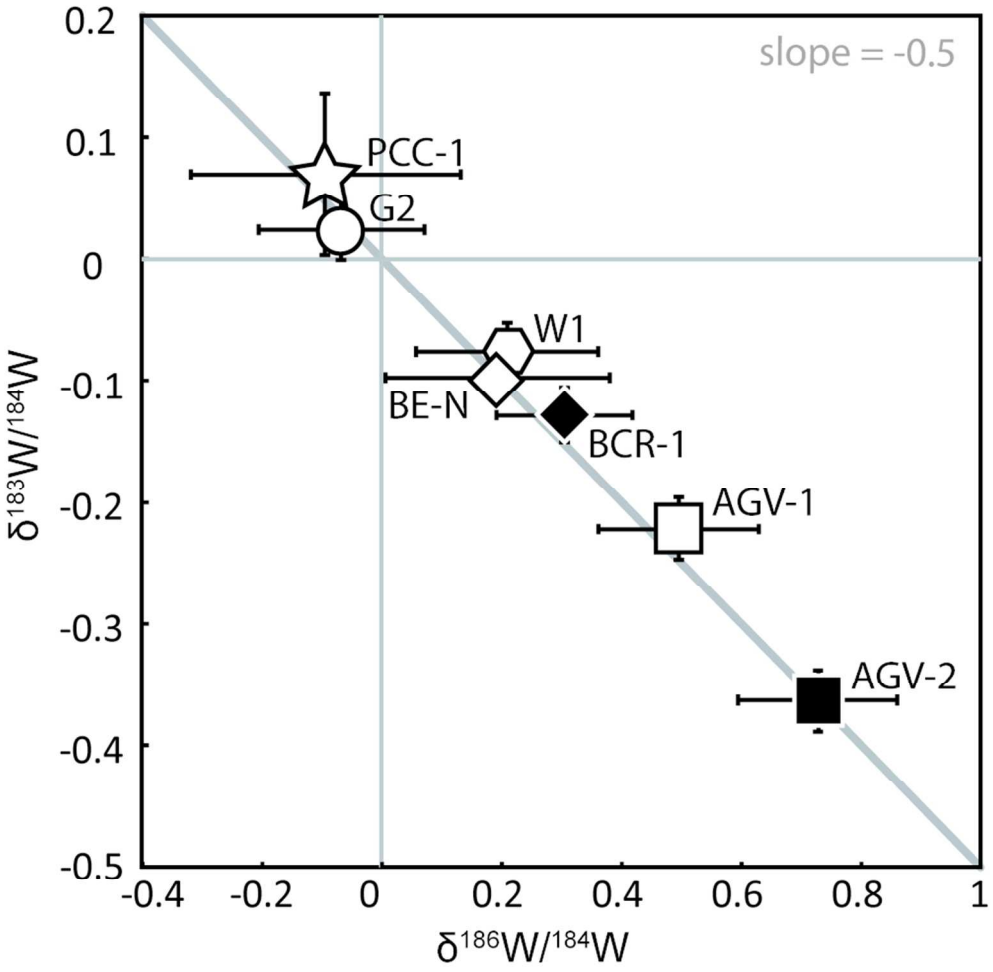

Figure 8
85x83mm (300 x 300 DPI)

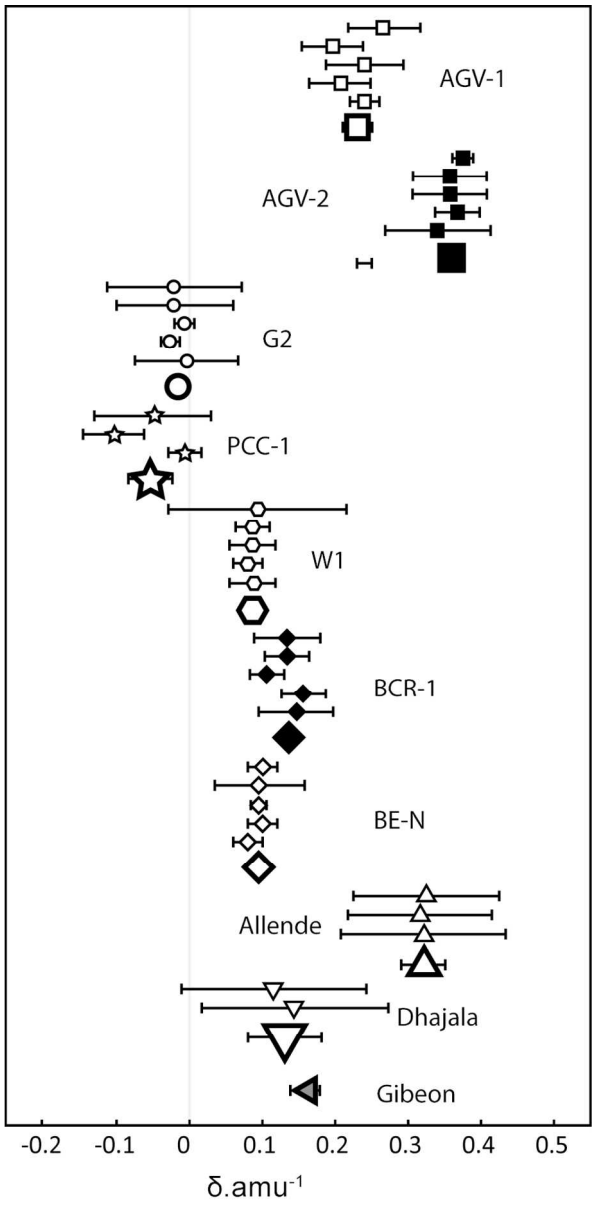

Figure 9
79x162mm (300 x 300 DPI)